crystals

MDPI

Article

Mechanical Property and Corrosion Behavior of Powder-Metallurgy-Processed 3D Graphene-Networks-Reinforced Al Matrix Composites

Meng Zeng, Hongmei Chen, Xiaoma Tao and Yifang Ouyang *

State Key Laboratory of Featured Metal Materials and Life-Cycle Safety for Composite Structures, School of Physical Science and Technology, Guangxi University, Nanning 530004, China; taoxiaoma@gxu.edu.cn (X.T.)
* Correspondence: ouyangyf@gxu.edu.cn

Abstract: Three-dimensional graphene networks (3DGN) have the potential to be used as a reinforcement for aluminum matrix composites due to their unique wrinkled structure and cost-effectiveness. In this work, the mechanical properties and corrosion resistance of 3DGN in Al matrix were systematically investigated. 3DGN/Al composites with weight ratios of 0, 0.075, 0.150, 0.225, and 0.300 3DGN were prepared by powder metallurgy following by ball mill and spark plasma sintering. Results revealed that the densification of 3DGN/Al composites slightly decreases with the increase of 3DGN content. Increased hardness without loss of ductility was recorded compared to the pure aluminum sample prepared under the same experimental conditions. 3DGN/Al composites exhibit higher corrosion currents density than that of pure aluminum, which shows that the addition of 3DGN reinforcement aggravates the corrosion of aluminum. This study can be used as a reference for future research on the effect of graphene on the various properties of graphene-reinforced aluminum matrix composites.

Keywords: aluminum matrix composites; 3-dimensional graphene networks; reinforcement; spark plasma sintering

check for updates

Citation: Zeng, M.; Chen, H.; Tao, X.; Ouyang, Y. Mechanical Property and Corrosion Behavior of Powder-Metallurgy-Processed 3D Graphene-Networks-Reinforced Al Matrix Composites. *Crystals* **2023**, *13*, 485. https://doi.org/10.3390/cryst13030485

Academic Editor: Tomasz Sadowski

Received: 13 February 2023
Revised: 7 March 2023
Accepted: 8 March 2023
Published: 11 March 2023

1. Introduction

Graphene is a two-dimensional (2D) carbon material composed of layers of sp^2 hybridized carbon atoms, which can be wrapped up into zero-dimensional (0D) Bucky balls, rolled into one-dimensional (1D) nanotubes (e.g., carbon nanotubes and carbon nanofibers), or stacked into three-dimensional (3D) materials [1]. With the increasing maturity of the graphene preparation process, increasing interest in the applications of graphene materials has focused on their use as a reinforcement [2]. Graphene's high Young's modulus (1 TPa), high fracture strength (130 GPa), ultra-large specific surface area (2630 m^2/g), low density (~2 g/cm^3), high thermal conductivity, and super electrical and tribological properties make it a tremendous reinforcement to metal matrix composites (MMCs) [3–6]. At present, there have been numerous reports published on graphene-reinforced MMCs [7]. It is believed that graphene materials primarily impact the physicochemical properties of MMCs through interfacial behavior, the types and fraction of reinforcements, and layered structure [8]. This is why graphene is superior to other reinforcements, such as TiC [9], TiB_2 [10], Al_2O_3 [11], etc. MMCs are developing towards ultra-lightweight, wear resistance, and chemical resistance [12]. In MMCs, aluminum matrix composites (AMCs) possessing low density, superior strength, high wear resistance, and high modulus have been used in the automotive, aerospace, defense, and military fields [13–15]. As a structural material, how to further improve the strength and corrosion resistance of AMCs is an increasingly important research topic. The superior properties of graphene materials may provide insight into the solution to this problem [16]. Park et al. reported carbon-nanotube-reinforced

AMCs with an improvement of 60% and 23% in the yield strength and tensile strength, respectively [17]. A study by Xie et al. showed that graphene-nanosheet-reinforced AMCs exhibited a 293.3% increase in strength with almost no loss in ductility [18]. Xie et al. obtained graphene-nanoplatelets-reinforced AMCs with long-term corrosion resistance in a chlorine-containing environment by uniformly dispersing graphene nanoplatelets in an aluminum matrix [19]. The incorporation of graphene materials into aluminum matrix shows great potential for the development of light and strong AMCs.

The type of graphene material incorporated into AMCs is of importance. In the past decade, the most widely used reinforcements of graphene material reinforcements in AMCs are 1D carbon nanotubes and 2D graphene nanosheets. However, 3D graphene material is rising and expected to be a potential graphene material due to its easy preparation compared to single-layer graphene, unique wrinkled structure, and economical cost. It is considered a new type of reinforcement capable of structural stability and hydrophobicity while keeping the large specific surface area and good electrical conductivity of graphene [20]. There are many studies on the use of 1D and 2D graphene materials in AMCs, as mentioned above. However, there are quite a few reports on the application of 3D graphene materials in other MMCs [21]. For example, Algul et al. [22] prepared 3D graphene–nickel matrix composites with higher wear resistance and lower friction coefficient than the nickel matrix, attributed to the solid lubrication effect of graphene. The 3D graphene–copper matrix composites reported by Chen et al. [23] had a yield strength and tensile strength of 290 MPa and 308 MPa, respectively, and the structure of 3D graphene was well preserved in the bulk composites. The successful application and enhancing effect of 3D graphene materials on MMCs encouraged us to investigate the effect of 3D graphene in 3D graphene-materials-reinforced AMCs. Bastwros et al. [24] have successfully prepared graphene-nanoflakes (few layers of graphene thickness)-reinforced AMCs and found a 47% increase in flexural strength due to the addition of graphene. Moreover, the unique property advantages of 3D graphene materials for the mechanical properties and corrosion resistance of AMCs deserve further study. In order to better understand the effect of 3D graphene materials as a reinforcement in AMCs, it is promising to study the effect of 3D graphene materials on the properties of AMCs.

As for the second problem associated with the effect of reinforcements for graphene materials reinforced AMCs, the percentage of graphene is quite essential for graphene-reinforced AMCs. Generally speaking, as the percentage increases continuously, wettability and dispersion decrease with subsequent agglomeration, leading to decreased properties. Yan et al. investigated the effect of different contents of graphene nanoflakes (GNFs) (0.15 and 0.50 wt%) on the mechanical properties of GNFs/Al composites and found that both tensile strength and yield strength increased significantly with the increasing GNF content [25]. Li et al. also prepared graphene nano-platelets (GNPs)-reinforced AMCs with contents of 0.4 wt% and 2 wt.%, respectively, and found that GNPs were uniformly distributed with strong interfacial bonding and significant load transfer in 0.4 wt% GNPs/Al composites. However, the tensile strength and ductility of 2 wt% GNPs/Al composites decreased due to the GNP aggregation [26]. Yolshina et al. prepared graphene-reinforced AMCs and graphite-reinforced AMCs with different proportions and found that graphene materials affect the corrosion resistance of the composites and accelerate the corrosion rate as the graphene materials content increases [27]. These results suggest that graphene content is also a key factor affecting the performance of AMCs. To date, most studies on graphene-reinforced AMCs have concentrated on low content of graphene (below 5 wt%) [28–30]. However, the atomic percentage is still large due to the low mass of the carbon atom. Many researchers believe that the optimal value of graphene is between 0.3–1.0 wt% [16], and it seems to be an interesting topic to further investigate the effect of content for graphene.

Additionally, the production process is extremely critical [31,32]. Palei et al. used powder metallurgy (PM) to fabricate graphene-reinforced AMCs and found graphene was in bi-layer form in the best graphene-reinforced AMCs [33]. Chen et al. prepared carbon-nanotubes-reinforced AMCs by using PM, which effectively improved the interfacial strength of AMCs, thus improving the load transfer efficiency [34]. Ujah and Chen also considered that PM was the most effective solid fabrication method for producing AMCs [35,36]. The main process of PM is: preparation and preparation of raw materials, obtaining green compact, sintering, and forming [37]. Jiang et al. observed that ball mill (BM) with a speed of 200 r/min was the most favorable speed to achieve uniform dispersion maximization without destructively damaging the original structure of graphene [38]. High-temperature sintering can usually deteriorate the mechanical property of AMCs and result in the formation of metallic carbide, such as Al_4C_3, which is a brittle phase and highly susceptible to hydrolysis, which is not conducive to the existence of AMCs in humid environments, thus adversely affecting the corrosion resistance performance of AMCs [39]. In recent decades, due to rapid sintering and low sintering temperature (which is less likely to produce intergranular compounds), spark plasma sintering (SPS) technology has been widely used for simultaneous heating and sintering of pressed powders and is regarded as the best sintering technique in AMCs [35,40–43].

In our previous work [44], we successfully prepared AMCs using the BM and SPS technique and found that 3D graphene networks (3DGN) were efficiently distributed in the aluminum matrix and no carbide phase was detected, which could negatively impact corrosion resistance. Therefore, this work aims to explore the PM method with BM and SPS to prepare 3DGN/Al composites, and to investigate the effect of different 3DGN contents on the mechanical properties and corrosion resistance performance of graphene-reinforced aluminum matrix composites.

2. Materials and Methods

2.1. Materials

Pure aluminum (99.99%) with nominal particle size smaller than 48 μm purchased from Beijing Ryubon New Material Co., Ltd., Beijing, China, was selected as matrix material. Al particles are close to spherical shapes with variable sizes, as shown in Figure 1a. Furthermore, 3DGN, supplied by Guangxi University Graphene Energy Center, China, was selected as reinforcement. As shown in Figure 1b, the morphology of 3DGN was assessed through field emission scanning electron microscope (SEM, Sigma-500 Zeiss, Oberkochen, Germany). One can see that 3DGN with different sizes of flake-like shapes and wrinkled structure is semi-transparent, which means it is very thin.

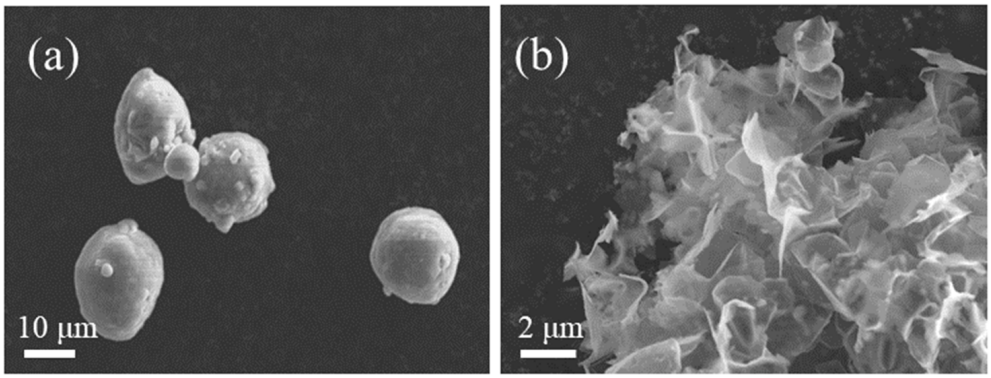

Figure 1. SEM morphologies of the raw materials (**a**) aluminum and (**b**) 3DGN.

2.2. Preparation of Composites

To enable better dispersion of 3DGN in aluminum matrix, first, 3DGN was dispersed in anhydrous ethanol and sonicated for 30 min to obtain 3DGN solution. Aluminum particles are mixed with 3DGN solution, the weight percentage of 3DGN in the aluminum matrix was maintained at 0.075, 0.150, 0.225 and 0.300 to obtain different 3DGN/Al composites solution. A pure aluminum sample was prepared for comparison. All specimens were poured into a planetary ball mill for milling two hours, under a rotational speed of 200 r/min. The ball to powder was kept as 20:1, and nitrogen as protective gas. After milling, the mixed solution was transferred to a vacuum drying oven for drying to obtain the mixed powders. Dried mixed powders were pre-compacted into green compact at room temperature and then transferred to a furnace sintered by using spark plasma sintering (SPS, LABOX-225, Sinter Land, Niigata, Japan). The sintering was performed at a heating rate of 100 °C per minute up to 600 °C and hold at 600 °C for 10 min. The process of sintering was carried out under the vacuum atmosphere and the pressure of 50 MPa. Eventually, sintered samples were characterized and evaluated for the mechanical and corrosion resistance properties.

2.3. Mechanical and Corrosion Resistance Characterization

X-ray diffraction analysis (XRD, SMARTLAB 3kW, Rigaku, Tokyo, Japan) was employed to detect the different phases present in raw Al, 3DGN and 3DGN/Al composite powders and fabricated 3DGN/Al composites after BM and SPS process. Theoretical density of 3DGN/Al composites with different 3DGN contents was calculated by the rule of mixture [45]. The experimental density of sintered pure aluminum and 3DGN/Al composites samples was determined using the Archimedean method. The experimental density as a percentage of the theoretical density is the relative density, which can be used to characterize the densification [46]. The Vickers hardness (HV) of the developed composites was tested by a hardness tester (HWDM-3) at a test load of 9.8 N and dwell time of 10 s. The average hardness values of five sets for each sample were evaluated to ensure the accuracy of the results. A universal loading machine (INSTRON-8801, Instron, Canton, MA, USA) was used to test the compression properties. Finally, the corrosion resistance properties of all samples in 3.5 wt.% NaCl solution were studied in an electrochemical potentiostat (Reference-600, Gamry Instruments, Warminster, PA, USA) at ambient temperature. A three-electrode cell was used with a saturated calomel electrode (SCE) as a reference and a platinum mesh as the counter electrode (CE). The corrosion cell of 1 cm^2 was used as working surface. The impedance measurements were performed with an AC signal amplitude of 5 mV rms, 10 points/decade and a frequency range of 0.01 Hz–100,000 Hz. Tafel curve was recorded from corrosion potential (E_{corr}) −0.2 V to E_{corr} +0.2 V, with scan rate 1 mV/s. The E_{corr} and corrosion current density (I_{corr}) were obtained by fitting the experimental data to Tafel curve.

3. Results and Discussion

3.1. Microstructure

Figure 2 shows the XRD patterns of raw aluminum powder and raw 3DGN. The characteristic XRD peaks of aluminum (space group is Fm-3m (225), 2θ [111] = 38.4°, 2θ [200] = 44.7°, 2θ [220] = 65.4°, 2θ [331] = 78.2°, 2θ [222] = 82.4°) can been seen in Figure 2a, indicating that it is relatively pure aluminum and no other impurities are detected. Diffraction peaks at 26° and 43° of typical graphene structure can be seen in the XRD pattern of raw 3DGN, consistent with the graphene XRD results reported by Şenel et al. [3]. The XRD patterns of these raw powders are essential for the detection of the phase structure in the prepared 3DGN/Al composites.

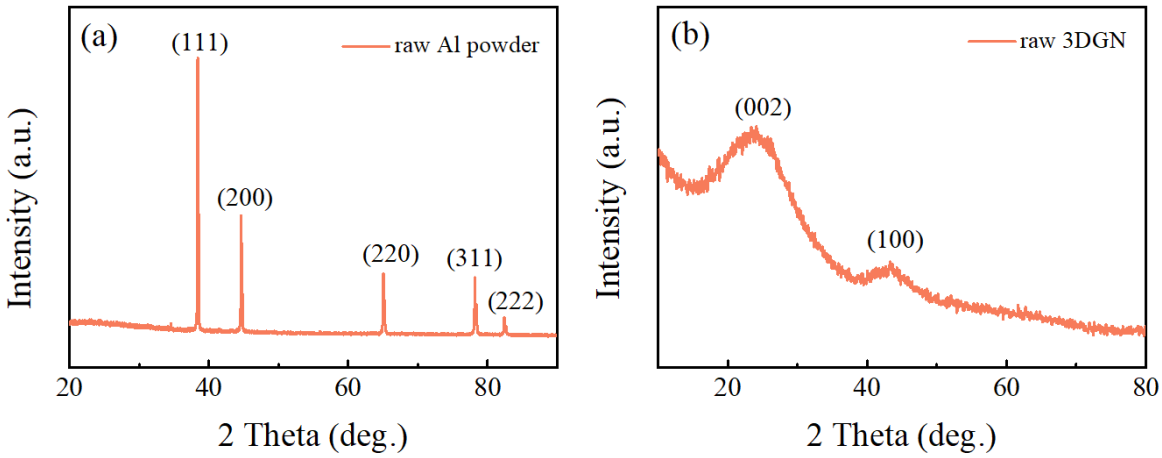

Figure 2. XRD spectra of raw materials (**a**) Al powder and (**b**) 3DGN.

XRD of all prepared 3DGN/Al composites samples are shown in Figure 3. Typical diffraction peaks corresponding to aluminum can been seen. However, no diffraction peaks related to 3DGN could be observed in the 3DGN/Al composites because the 3DGN in 0.3 wt% addition is smaller than the detection limit of XRD diffractometer [24]. From Figure 3, one cannot observe any obvious shift of the positions for aluminum diffraction peaks; this means that there is no apparent solution of carbon in aluminum. Furthermore no aluminum oxide or aluminum carbides were detected; similar results were obtained by Chen et al. [34]. We cannot conclude that no aluminum oxide or aluminum carbides were produced during the sintering process, but we can assume that the oxidation reaction and interfacial reaction are not significant or that the content of impurity phases, such as alumina and aluminum carbide, is extremely marginal.

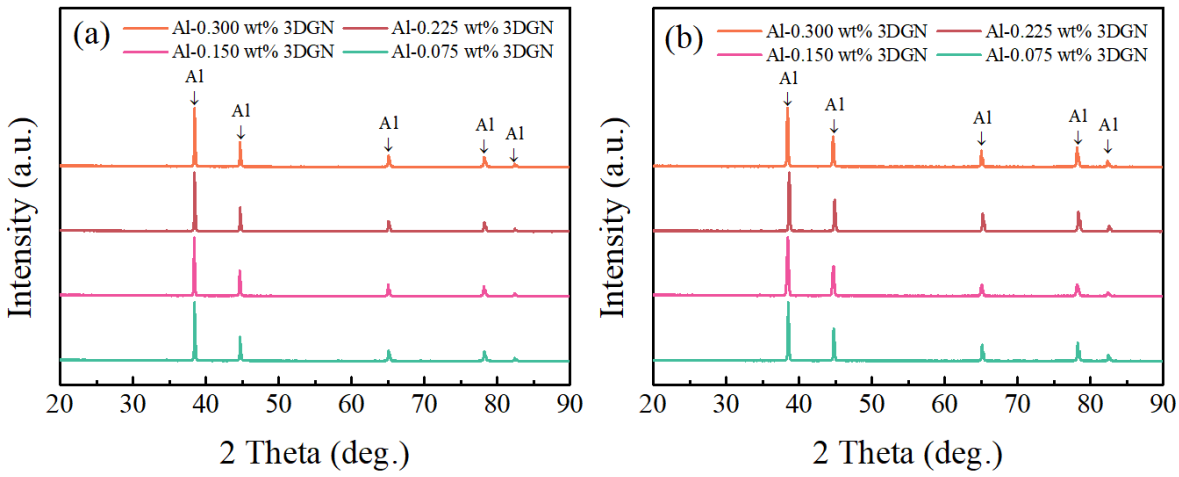

Figure 3. XRD patterns of fabricated (**a**) 3DGN/Al composite powders and (**b**) sintered 3DGN/Al composites.

Figure 4 illustrates the microstructure of ball-milled pure aluminum specimen and ball-milled 3DGN/Al composite powders. It can be seen from Figure 4a that after ball milling, pure aluminum powder changed from spherical shape to flakes or was crushed into powder agglomerate due to aggregation. This flake-like aluminum is favorable because it can provide more sites than agglomeration for 3DGN attachment. As depicted in Figure 4b,c, 3DGNs were mainly attached on the surface of the flake-like aluminum (identified with green arrows) and kept the original wrinkled structure, which indicates the effective distribution of 3DGN in 3DGN/Al composite powders and the possibility of producing a cohesive link between 3DGN and aluminum. The two most critical factors for the

preparation of 3DGN/Al composites are precisely the dispersion and the structural stability of 3DGN. Intriguingly, a piece of 3DGN was observed in Figure 4d,e, which was not found in the other 3DGN/Al composite powders. The presence of large pieces of 3DGN is evidence of 3DGN agglomeration. That is to say, 0.075%-3DGN/Al composite powders and 0.150%-3DGN/Al composite powders achieved homogeneous distribution of 3DGN, while 0.225% and 0.300% 3DGN were achieved in 3DGN/Al composite powders with some extent of agglomeration.

The morphologies of sintered pure Al sample and 3DGN/Al composites with different 3DGN contents and the EDS mapping analysis of 3DGN/Al composites with 0.300% 3DGN are given in Figure 5. All sintered specimens were nearly smooth and dense. A very small number of pores (as marked in Figure 5) appear on the surface of pure aluminum specimen in Figure 5a, indicating obviously that pure aluminum specimen is the densest. From Figure 5b,c, one can see that pores increase with the increasing addition of 3DGN. A more detailed observation of Figure 5d,e reveals that the large pores were formed by several small pores connected together. The 3DGN agglomeration mentioned above may also lead to the formation of porosity. In addition, the apparent morphologies of Figure 5d,e differ from those of Figure 5a–c, in which some gray or dark areas (already marked with red arrows) are observed. Further EDS analysis and elemental mapping of the gray or dark areas of 0.300%-3DGN/Al composites sample were performed and are shown in Figure 5f. The distribution of carbon element (shown in Figure 5f_1) and aluminum element (shown in Figure 5f_2) demonstrate that the gray or dark areas result from 3DGN agglomeration. Therefore, it can be inferred that the gray or dark areas of 0.225%-3DGN/Al composites sample in Figure 5d also result from the 3DGN agglomerations, though they are not as distinct as in Figure 5e. This inference is also consistent with the aforementioned statements that the morphology of large 3DGN agglomerates was observed only in both of 0.225%-3DGN/Al and 0.300%-3DGN/Al composite powders.

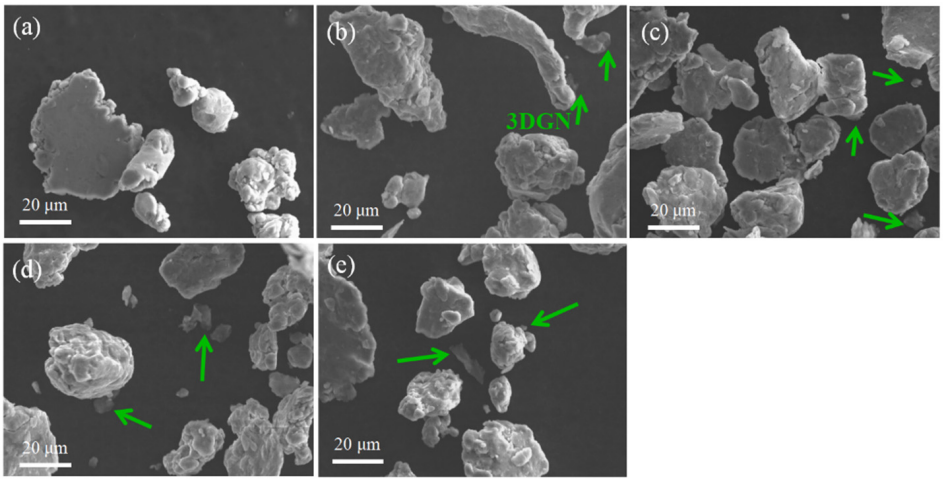

Figure 4. SEM images of (**a**) ball-milled pure Al powder, (**b**) ball-milled 0.075%-3DGN/Al composite powders, (**c**) ball-milled 0.150%-3DGN/Al composite powders, (**d**) ball-milled 0.225%-3DGN/Al composite powders, and (**e**) ball-milled 0.300%-3DGN/Al composite powders. The green arrows indicate the distribution of 3DGN.

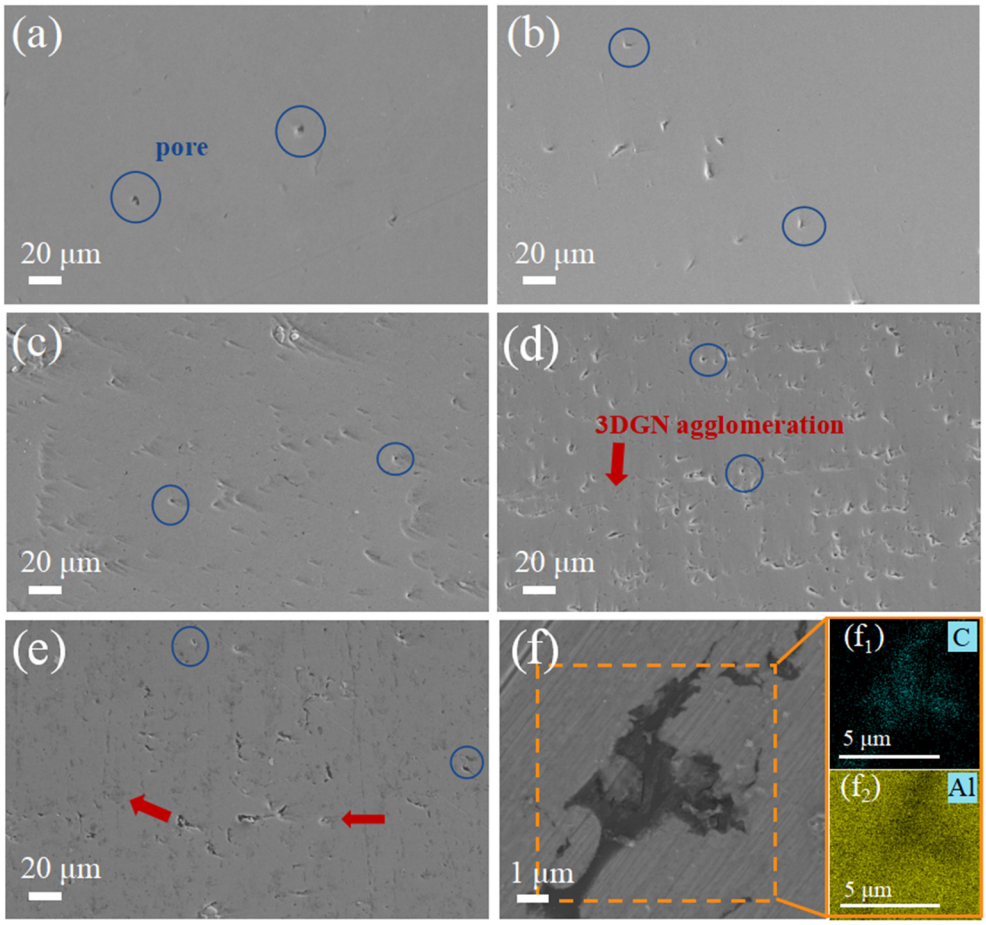

Figure 5. SEM images of (**a**) sintered pure Al sample, (**b**) sintered 0.075%-3DGN/Al composites, (**c**) sintered 0.150%-3DGN/Al composites, (**d**) sintered 0.225%-3DGN/Al composites, and (**e**) sintered 0.300%-3DGN/Al composites. (**f**), (**f$_1$**,**f$_2$**) EDS mapping analysis images of the sintered 0.300%-3DGN/Al composites. The blue circles and red arrows indicate the pore and 3DGN agglomeration, respectively.

3.2. Mechanical Property

Figure 6 shows the variation of theoretical density, experimental density, and relative density of the sintered pure Al sample and sintered 3DGN/Al composites. A decrease in the theoretical density with increasing 3DGN content can be seen; because 3DGN (2.22 g/cm^3) is lighter than pure aluminum (2.697 g/cm^3), it tends to reduce the bulk density of 3DGN/Al composites. The experimental density values of the sintered 3DGN/Al composites are all lower than that of the theoretical value. The relative density is over 97%, but density slightly decreases with the increase in 3DGN content, which is in good agreement with previous microstructure results. Similar results were also obtained by Liu et al. [47]. A monotonous decrease in relative density is related to the agglomeration associated with the increase in 3DGN content. This also can be explained by the fact that when the temperature is 600 °C, aluminum has a high viscosity, which can lead to poor liquid aluminum flow, resulting in the formation of pores [28].

It can be observed from Figure 7 that the Vickers hardness of prepared composites increases from 35.7 HV (pure aluminum sample) to 40.5 HV after the addition of 0.225 wt% 3DGN, which is higher than that obtained by Khanna et al. [29]. The improved mechanical properties of 3DGN/Al composites can be attributed to three factors: interfacial reaction, matrix grain refinement, and dislocation strengthening mechanism. First, graphene, with a high specific surface area of 2630 m^2/g, can shroud most of the aluminum powder particles, which facilitates increasing the intensity of the Al–C bond. This stronger Al–C interaction

provides the Al matrix additional chemical forces and strengthens the adhesion between Al and graphene, which is reflected in the increased hardness [33]. Second, BM process and the addition of 3DGN refined the aluminum grains, thus increasing the grain boundary, which can prevent the movement of the dislocations in the matrix material. Finally, as the sintering temperature increases, the thermal stress leads to the formation of dislocations at the matrix–reinforcement interface due to a thermal expansion mismatch between the aluminum matrix and the 3DGN reinforcement [16]. However, further addition of 3DGN is detrimental to the Vickers hardness. This is most likely due to the fact that excess 3DGN will agglomerate in the matrix, leading to fine porosity and decreased mechanical properties. On the other hand, the presence of van der Waals forces between 3DGN will cause layer-to-layer slip [29].

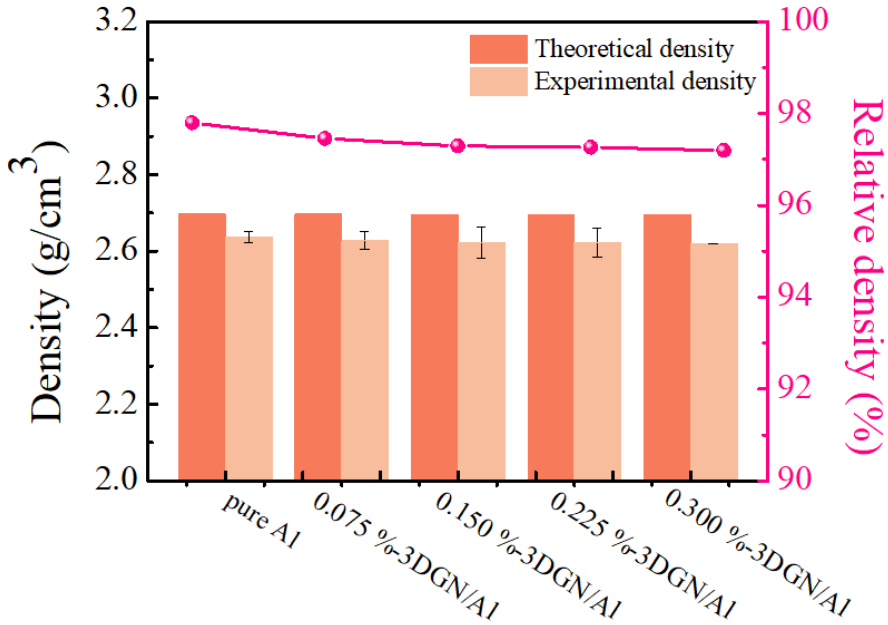

Figure 6. Theoretical density, experimental density, and relative density of pure Al and 3DGN/Al composites.

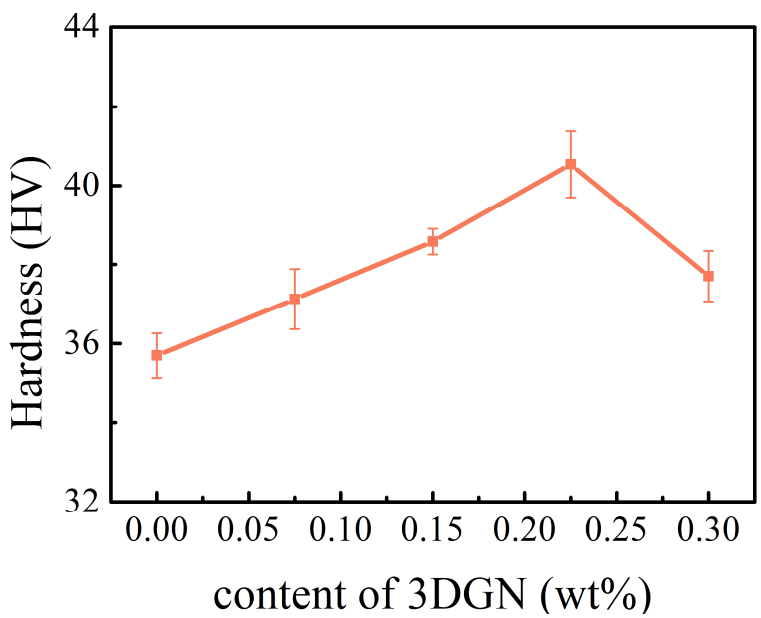

Figure 7. Vickers hardness of the bulk 3DGN/Al composites with different 3DGN contents.

Typical compressive strength curves of the prepared composites are shown in Figure 8. All 3DGN/Al composites exhibited the same favorable toughness as pure aluminum. It is generally expected that an increase in hardness leads to brittle deformation. However, the addition of 3DGN to aluminum matrix not only increased the hardness of the 3DGN/Al composites, but also maintained the good ductility. This unique mechanical property of 3DGN/Al composites can be explained for several reasons. Initially, 3DGN has a larger specific surface area than carbon nanotubes, carbon nanosheets, and other carbon materials [8], making it more possible to form Al–C bonds, which is beneficial for the transfer of external forces from aluminum to 3DGN. Additionally, in the process of stressing the composites material, 3DGN has a fold flattening and then fracture process due to its wrinkled structure, which gives the 3DGN/Al composites material excellent toughness [25]. Finally, 3DGN itself has strong tensile strength and good plasticity, and no metallic carbide in the interface between the matrix and reinforcements results in the overall ductility of the 3DGN/Al composites.

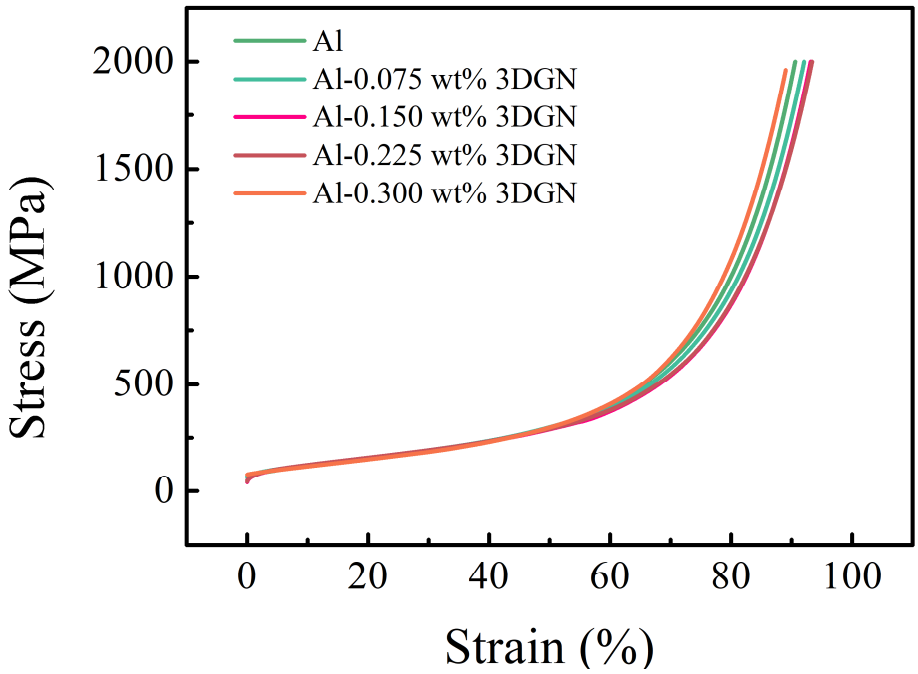

Figure 8. Compressive curves of the bulk 3DGN/Al composites with different 3DGN contents.

3.3. Corrosion Resistance Performance

The corrosion resistance properties are characterized by impedance and polarization tests. The Nyquist curves and Tafel polarization curves of 3DGN/Al composites are presented in Figure 9. The E_{corr} and I_{corr} obtained from the polarization curve are shown in Table 1. The Nyquist curve is usually a semicircle or several interconnected semicircles and is often applied to determine the stability of a system. The diameters of Nyquist curves of all 3DGN/Al composites are significantly larger than those of the referenced pure aluminum sample in Figure 9a. This result indicates that the long-term corrosion resistance stability of 3DGN/Al composites in 3.5 wt% NaCl solution gradually increases as the content of 3DGN increases to 0.150 wt%. This is because the Nyquist curves are related to the electrode–electrolyte interface. The hydrophobicity of 3DGN will certainly have a positive effect on the contact interface between Al and the corrosion solution, thus favoring the increase of the Nyquist curves [48]. Then, excess 3DGN makes the Nyquist radii deteriorate. This obviously has a significant relationship with the fact that 3DGN agglomeration occurs, as mentioned above, when the 3DGN content varies from 0.225% to 0.300% and the 3DGN agglomeration becomes progressively more severe. Thus, the barrier

effect of blocking the contact between Al and corrosion solution decreases and the good electrical conductivity of 3DGN itself may also reduce the corrosion resistance stability.

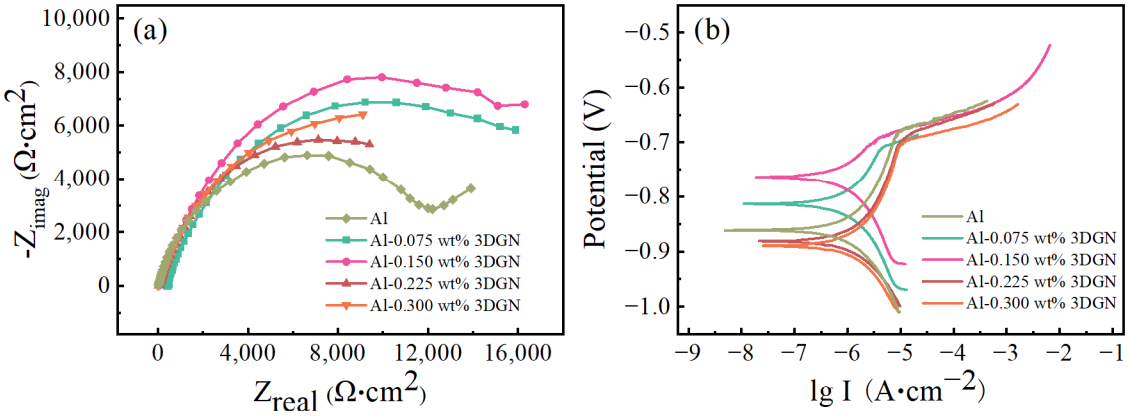

Figure 9. (**a**) Nyquist plots of 3DGN/Al composites and (**b**) potentiodynamic polarization curves of 3DGN/Al composites.

Table 1. Corrosion potential (E_{corr}) and corrosion current density (I_{corr}) of the referenced pure aluminum sample and 3DGN/Al composites.

Sample	E_{corr} (mV)	I_{corr} (μA/cm^2)
Al	−861.4	2.456
Al-0.075 wt% 3DGN	−813.6	3.031
Al-0.150 wt% 3DGN	−763.8	2.608
Al-0.225 wt% 3DGN	−881.4	3.151
Al-0.300 wt% 3DGN	−889.5	3.582

Figure 9b shows that all prepared pure Al and 3DGN/Al composites samples show a state of passivation, which is explained by the fact that once the aluminum matrix is broken through, it is extremely easy to develop an oxide film or corrosion product layer, thus preventing further corrosion. One can see that the breakdown onset of the passive films of the 3DGN/Al composites is lower than that of pure aluminum, implying that the pitting resistance and the pitting susceptibility of pure aluminum are the highest, while the pitting resistance and the pitting susceptibility of the 3DGN/Al composites become inferior. The E_{corr} and I_{corr} are used to characterize the corrosion resistance of each 3DGN/Al composite. One can see that the changes of E_{corr} and I_{corr} are non-linear. Even with a small amount of 3DGN addition, the E_{corr} of 0.075 wt% and 0.150 wt% 3DGN/Al composites is higher than that of the referenced pure aluminum. In addition, 3DGN/Al composites with 0.150 wt% have the highest E_{corr}, implying that is they are the most difficult to be corroded thermodynamically among all 3DGN/Al composites samples. This is consistent with the results shown in Figure 9a, in which 3DGN/Al composites with 0.150 wt% 3DGN exhibits the greatest resistance to corrosion. However, the I_{corr} of all 3DGN/Al composites is higher than that of the pure aluminum sample, which is in good agreement with the corrosion study results of pure aluminum and graphene-reinforced aluminum composites by Yolshina et al. [27]. The 3DGN/Al composites with lower densification than that of pure aluminum are one of the reasons for the higher I_{corr} [49]. The porosity and crevices between the interface of aluminum matrix and 3DGN reinforcement are favorable sites for pitting of metals in AMCs and accelerating the dissolution of aluminum matrix [50]. Furthermore, aluminum oxide is very dense, which can prevent further corrosion. In contrast, 3DGN is a loosely layered structure, and some 3DGNs dispersed in the aluminum matrix result in the local destruction of the continuity of the aluminum oxide. This increases the number of corrosion sites and brings about the conditions for further corrosion and propagation in the aluminum matrix [51]. As for 3DGN/Al composites, the aluminum matrix is an anode,

and 3DGN is a cathode, and the galvanic corrosion occurs in the electrolyte. The galvanic corrosion continues to increase the forward potential, which leads to an increase in the current density of the anodic reaction.

4. Conclusions

In this work, a pure aluminum sample and 3DGN/Al composites with 3DGN weight percentages of 0.075, 0.150, 0.225, and 0.300 were prepared using a powder metallurgy technique with BM and SPS. The mechanical and corrosion-resistance properties were examined, and the results indicate that the relative density of 3DGN/Al composites keeps more than 97%, but decreases with the increase of 3DGN content. The addition of 3DGN results in a slight increase in hardness of 3DGN/Al composites compared with pure aluminum, while the ductility remains unchanged. The hardness of 3DGN/Al composites is gradually increased with increase in the content of 3DGN, reaching a maximum at 0.225 wt% 3DGN, and then decreases. In other words, the effect of 0.075%~0.300% 3DGN contents in 3DGN/Al composites on mechanical properties depends on the content of 3DGN. Meanwhile, the corrosion rate of 3DGN/Al composites is higher than that of the initial pure aluminum specimen, indicating that 3DGN can negatively impact the corrosion resistance performance of 3DGN/Al composites. These results demonstrate that the 3DGN has different effects on mechanical properties and corrosion resistance performance of AMCs. This study demonstrates that the addition of graphene materials improves the mechanical properties of AMCs but brings about the negative impacts of graphene materials in terms of corrosion resistance. These results may be used as a reference for selecting the appropriate amount of graphene for different properties in graphene-reinforced aluminum matrix composites, and also supports the potential application of low-content graphene-reinforced composites.

Author Contributions: M.Z.: conceptualization, investigation, experiment, formal analysis, writing—original draft. H.C.: formal analysis, writing—review and editing. X.T.: formal analysis, writing—review and editing, funding acquisition. Y.O.: conceptualization, supervision, writing—review and editing, funding acquisition. All authors have read and agreed to the published version of the manuscript.

Funding: This research was funded by the National Natural Science Foundation of China grant number [11964003, 51961007], and funded by the Guangxi Natural Science Foundation grant number [2018GXNSFAA281291, 2018GXNSFAA281254].

Acknowledgments: The authors would like to express deep gratitude to Professor Zhiqun Tian for providing three-dimensional graphene for this study.

Conflicts of Interest: The authors declare no conflict of interest.

References

1. Tjong, S.C. Recent progress in the development and properties of novel metal matrix nanocomposites reinforced with carbon nanotubes and graphene nanosheets. *Mater. Sci. Eng. R-Rep.* **2013**, *74*, 281–350. [CrossRef]
2. Goyat, R.; Saharan, Y.; Singh, J.; Umar, A.; Akbar, S. Synthesis of graphene-based nanocomposites for environmental remediation applications: A review. *Molecules* **2022**, *27*, 6433. [CrossRef] [PubMed]
3. Şenel, M.C.; Gürbüz, M.; Koç, E. Fabrication and characterization of synergistic Al-SiC-GNPs hybrid composites. *Compos. Part B Eng.* **2018**, *154*, 1–9. [CrossRef]
4. Berman, D.; Erdemir, A.; Sumant, A.V. Graphene: A new emerging lubricant. *Mater. Today* **2014**, *17*, 31–42. [CrossRef]
5. Su, Y.; Li, Z.; Yu, Y.; Zhao, L.; Li, Z.; Guo, Q.; Xiong, D.; Zhang, D. Composite structural modeling and tensile mechanical behavior of graphene reinforced metal matrix composites. *Sci. China-Mater.* **2017**, *61*, 112–124. [CrossRef]
6. Moustafa, E.B.; Abushanab, W.S.; Melaibari, A.; Yakovtseva, O.; Mosleh, A.O. The effectiveness of incorporating hybrid reinforcement nanoparticles in the enhancement of the tribological behavior of aluminum metal matrix composites. *JOM* **2021**, *73*, 4338–4348. [CrossRef]
7. Hu, Z.; Tong, G.; Lin, D.; Chen, C.; Guo, H.; Xu, J.; Zhou, L. Graphene-reinforced metal matrix nanocomposites—A review. *Mater. Sci. Technol.* **2016**, *32*, 930–953. [CrossRef]
8. Zemtsova, E.G.; Arbenin, A.Y.; Sidorov, Y.V.; Morozov, N.F.; Korusenko, P.M.; Semenov, B.N.; Smirnov, V.M. The use of carbon-containing compounds to prepare functional and structural composite materials: A review. *Appl. Sci.* **2023**, *12*, 9945. [CrossRef]

9. Li, S.-S.; Zhang, H.; Chang, F.; Fei, Y.-N.; Kou, S.-Q.; Shao, Y.; Xuan, Q.-Q.; Li, X.; Qiu, F. Effects of alloy elements (Mg, Zn) on the microstructure and mechanical properties of (TiC+TiB_2)/Al composites. *Ceram. Int.* **2022**, *48*, 22096–22105. [CrossRef]
10. Liu, Z.; Zhu, T.; Jia, Y.; Song, D.; Zhou, N.; Zheng, K. Preparation of in-situ TiB_2 reinforced aluminum matrix composites assisted by two steps of ultrasonic vibration. *Mater. Res. Express* **2021**, *8*, 046506. [CrossRef]
11. Ic, Y.T.; Güler, E.S.; Sezer, B.; Taş, B.S.; Şahin, H.S. Multi-objective optimization of turning parameters for SiC- or Al_2O_3-reinforced aluminum matrix composites. *Process Integr. Optim. Sustain.* **2021**, *5*, 609–623. [CrossRef]
12. Ashebir, D.A.; Mengesha, G.A.; Sinha, D.K.; Mohan, D.G. An insight into mechanical and metallurgical behavior of hybrid reinforced aluminum metal matrix composite. *Adv. Mater. Sci. Eng.* **2022**, *2022*, 7843981. [CrossRef]
13. Ghahremani, A.; Abdullah, A.; Fallahi Arezoodar, A. Wear behavior of metal matrix nanocomposites. *Ceram. Int.* **2022**, *48*, 35947–35965. [CrossRef]
14. Kumar, V.M.; Venkatesh, C.V. A comprehensive review on material selection, processing, characterization and applications of aluminium metal matrix composites. *Mater. Res. Express* **2019**, *6*, 072001. [CrossRef]
15. Narhari Tekale, S.; Dolas, D.R. Study of fabrication methods and various reinforcements with aluminium for automotive application—A review. *Mater. Today Proc.* **2022**, *62*, 2768–2773. [CrossRef]
16. Md Ali, A.; Omar, M.Z.; Hashim, H.; Salleh, M.S.; Mohamed, I.F. Recent development in graphene-reinforced aluminium matrix composite: A review. *Rev. Adv. Mater. Sci.* **2021**, *60*, 801–817. [CrossRef]
17. Park, J.G.; Keum, D.H.; Lee, Y.H. Strengthening mechanisms in carbon nanotube-reinforced aluminum composites. *Carbon* **2015**, *95*, 690–698. [CrossRef]
18. Xie, Y.; Meng, X.; Chang, Y.; Mao, D.; Yang, Y.; Xu, Y.; Wan, L.; Huang, Y. Ameliorating strength-ductility efficiency of graphene nanoplatelet-reinforced aluminum composites via deformation-driven metallurgy. *Compos. Sci. Technol.* **2022**, *219*, 109225. [CrossRef]
19. Xie, Y.; Meng, X.; Mao, D.; Qin, Z.; Wan, L.; Huang, Y. Homogeneously dispersed graphene nanoplatelets as long-term corrosion inhibitors for aluminum matrix composites. *ACS Appl. Mater. Interfaces* **2021**, *13*, 32161–32174. [CrossRef] [PubMed]
20. Sun, H.; Xu, Z.; Gao, C. Multifunctional, ultra-flyweight, synergistically assembled carbon aerogels. *Adv. Mater.* **2013**, *25*, 2554–2560. [CrossRef]
21. Meng, F.; Wang, H.; Huang, F.; Guo, Y.; Wang, Z.; Hui, D.; Zhou, Z. Graphene-based microwave absorbing composites: A review and prospective. *Compos. B-Eng.* **2018**, *137*, 260–277. [CrossRef]
22. Algul, H.; Tokur, M.; Ozcan, S.; Uysal, M.; Cetinkaya, T.; Akbulut, H.; Alp, A. The effect of graphene content and sliding speed on the wear mechanism of nickel–graphene nanocomposites. *Appl. Surf. Sci.* **2015**, *359*, 340–348. [CrossRef]
23. Chen, Y.; Zhang, X.; Liu, E.; He, C.; Han, Y.; Li, Q.; Nash, P.; Zhao, N. Fabrication of three-dimensional graphene/Cu composite by in-situ CVD and its strengthening mechanism. *J. Alloys Compd.* **2016**, *688*, 69–76. [CrossRef]
24. Bastwros, M.; Kim, G.Y.; Zhu, C.; Zhang, K.; Wang, S.; Tang, X.; Wang, X. Effect of ball milling on graphene reinforced Al6061 composite fabricated by semi-solid sintering. *Compos. B-Eng.* **2014**, *60*, 111–118. [CrossRef]
25. Yan, S.J.; Dai, S.L.; Zhang, X.Y.; Yang, C.; Hong, Q.H.; Chen, J.Z.; Lin, Z.M. Investigating aluminum alloy reinforced by graphene nanoflakes. *Mater. Sci. Eng. A* **2014**, *612*, 440–444. [CrossRef]
26. Li, J.; Zhang, X.; Geng, L. Improving graphene distribution and mechanical properties of GNP/Al composites by cold drawing. *Mater. Des.* **2018**, *144*, 159–168. [CrossRef]
27. Yolshina, L.A.; Muradymov, R.V.; Molchanova, N.G. Corrosion behavior of aluminum–graphene and aluminum–graphite composite materials in a 3% NaCl aqueous solution. *Russ. Metall.* **2022**, *2022*, 153–160. [CrossRef]
28. Zhang, Y.; Zhu, G.; Gao, B.; Wang, L.; Li, Z.; Hu, L.; Shi, Z.; Yin, Q. Effect of high-current pulsed electron beam on properties of graphene-modified aluminum titanium carbide composites. *Materials* **2022**, *15*, 7879. [CrossRef] [PubMed]
29. Khanna, V.; Kumar, V.; Bansal, S.A. Effect of reinforcing graphene nanoplatelets (GNP) on the strength of aluminium (Al) metal matrix nanocomposites. *Mater. Today Proc.* **2022**, *61*, 280–285. [CrossRef]
30. Kwon, H.; Estili, M.; Takagi, K.; Miyazaki, T.; Kawasaki, A. Combination of hot extrusion and spark plasma sintering for producing carbon nanotube reinforced aluminum matrix composites. *Carbon* **2009**, *47*, 570–577. [CrossRef]
31. Shuang, F.; Dai, Z.; Aifantis, K.E. Strengthening in metal/graphene composites: Capturing the transition from interface to precipitate hardening. *ACS Appl. Mater. Interfaces* **2021**, *13*, 26610–26620. [CrossRef]
32. Podobová, M.; Puchý, V.; Falat, L.; Džunda, R.; Besterci, M. Waste metals based metal-matrix ceramic-reinforced composites for friction applications. *Kov. Mater.-Met. Mater.* **2022**, *60*, 351.
33. Palei, B.B.; Dash, T.; Biswal, S.K. Graphene reinforced aluminum nanocomposites: Synthesis, characterization and properties. *J. Mater. Sci.* **2022**, *57*, 8544–8556. [CrossRef]
34. Chen, B.; Shen, J.; Ye, X.; Imai, H.; Umeda, J.; Takahashi, M.; Kondoh, K. Solid-state interfacial reaction and load transfer efficiency in carbon nanotubes (CNTs)-reinforced aluminum matrix composites. *Carbon* **2017**, *114*, 198–208. [CrossRef]
35. Ujah, C.O.; Kallon, D.V.V. Trends in aluminium matrix composite development. *Crystals* **2022**, *12*, 1357. [CrossRef]
36. Chen, S.; Chen, G.; Gao, P.; Liu, C.; Wu, A.; Dong, L.; Huang, Z.; Ouyang, C.; Zhang, H. Elevated-temperature tensile deformation and fracture behavior of particle-reinforced PM 8009Al matrix composite. *Bull. Pol. Acad. Sci.-Tech. Sci.* **2021**, *69*, 138846.
37. Kishore, K.L.; Padal, K.T.B. Effect of graphene nano plateletson microstructural and wearbehavior of AA7075/Al_2O_3 nano composites. *Mater. Today Proc.* **2022**, *62*, 4424–4431. [CrossRef]

38. Jiang, Y.; Tan, Z.; Xu, R.; Fan, G.; Xiong, D.-B.; Guo, Q.; Su, Y.; Li, Z.; Zhang, D. Tailoring the structure and mechanical properties of graphene nanosheet/aluminum composites by flake powder metallurgy via shift-speed ball milling. *Compos. A-Appl. Sci. Manuf.* **2018**, *111*, 73–82. [CrossRef]
39. Yolshina, L.A.; Muradymov, R.V.; Korsun, I.V.; Yakovlev, G.A.; Smirnov, S.V. Novel aluminum-graphene and aluminum-graphite metallic composite materials: Synthesis and properties. *J. Alloys Compd.* **2016**, *663*, 449–459. [CrossRef]
40. Al-Aqeeli, N.; Abdullahi, K.; Hakeem, A.S.; Suryanarayana, C.; Laoui, T.; Nouari, S. Synthesis, characterisation and mechanical properties of SiC reinforced Al based nanocomposites processed by MA and SPS. *Powder Metall.* **2013**, *56*, 149–157. [CrossRef]
41. Latief, F.H.; Sherif, E.S.M. Effects of sintering temperature and graphite addition on the mechanical properties of aluminum. *J. Ind. Eng. Chem.* **2012**, *18*, 2129–2134. [CrossRef]
42. Kwon, H.; Park, D.H.; Silvain, J.F.; Kawasaki, A. Investigation of carbon nanotube reinforced aluminum matrix composite materials. *Compos. Sci. Technol.* **2010**, *70*, 546–550. [CrossRef]
43. Prakash, C.; Singh, S.; Sharma, S.; Garg, H.; Singh, J.; Kumar, H.; Singh, G. Fabrication of aluminium carbon nano tube silicon carbide particles based hybrid nano-composite by spark plasma sintering. *Mater. Today Proc.* **2020**, *21*, 1637–1642. [CrossRef]
44. Zeng, M.; Lin, K.; Zhou, Z.; Chen, H.; Tao, X.; Ouyang, Y.; Du, Y. Effects of 3D graphene networks on the microstructure and physical properties of SiC/Al composites. *Ceram. Int.* **2023**, *49*, 8140–8147. [CrossRef]
45. Khan, M.; Din, R.U.; Basit, M.A.; Wadood, A.; Husain, S.W.; Akhtar, S.; Aune, R.E. Study of microstructure and mechanical behaviour of aluminium alloy hybrid composite with boron carbide and graphene nanoplatelets. *Mater. Chem. Phys.* **2021**, *271*, 124936. [CrossRef]
46. Venkatesh, V.S.S.; Deoghare, A.B. Microstructural characterization and mechanical behaviour of SiC and Kaoline reinforced aluminium metal matrix composites fabricated through powder metallurgy technique. *Silicon* **2021**, *14*, 3723–3737. [CrossRef]
47. Liu, J.; Khan, U.; Coleman, J.; Fernandez, B.; Rodriguez, P.; Naher, S.; Brabazon, D. Graphene oxide and graphene nanosheet reinforced aluminium matrix composites: Powder synthesis and prepared composite characteristics. *Mater. Des.* **2016**, *94*, 87–94. [CrossRef]
48. Chen, Q.; Jiang, Z.; Tang, S.; Dong, W.; Tong, Q.; Li, W. Influence of graphene particles on the micro-arc oxidation behaviors of 6063 aluminum alloy and the coating properties. *Appl. Surf. Sci.* **2017**, *423*, 939–950. [CrossRef]
49. Akçamlı, N.; Küçükelyas, B.; Kaykılarlı, C.; Uzunsoy, D. Investigation of microstructural, mechanical and corrosion properties of graphene nanoplatelets reinforced Al matrix composites. *Mater. Res. Express* **2019**, *6*, 115627. [CrossRef]
50. Kondakci, E.; Solak, N. Enhanced thermal conductivity and long-term stability of diamond/aluminum composites using SiC-coated diamond particles. *J. Mater. Sci.* **2022**, *57*, 3430–3440. [CrossRef]
51. Rashad, M.; Pan, F.; Yu, Z.; Asif, M.; Lin, H.; Pan, R. Investigation on microstructural, mechanical and electrochemical properties of aluminum composites reinforced with graphene nanoplatelets. *Prog. Nat. Sci.* **2015**, *25*, 460–470. [CrossRef]